Radiative Capture and Neutron Emission in $La^{139}+\alpha$ and $Ce^{142}+p$*†

E. V. VERDIECK AND J. M. MILLER‡
Department of Chemistry, Columbia University, New York, New York
(Received 2 August 1966)

The excitation functions for the reactions $La^{139}(\alpha,\gamma)Pr^{143}$, $Ce^{142}(p,\gamma)Pr^{143}$, $La^{139}(\alpha,n)Pr^{142}$, and $Ce^{142}(p,n)Pr^{142}$ at excitation energies of 8–38 MeV have been measured. The excitation function of the (α,γ) reaction rises to about 75 μb at 17-MeV excitation energy and falls to about 10 μb at 28-MeV excitation energy. The excitation function of the (p,γ) reaction rises to about 650 μb at 19-MeV and falls to about 80 μb at 36-MeV excitation energy. The large difference both in the shapes and in the magnitudes at the maxima of the two excitation functions, despite the fact that both reactions proceed through the same compound system Pr^{143}, is evidence for a direct contribution to the radiative capture of protons. A calculation of the (α,γ) excitation function based upon the compound-nucleus model agrees reasonably well with the experimental results, while a direct-interaction calculation of the (p,γ) reaction, although not in good agreement with the experimental results, gives a substantially better agreement than one within the compound-nucleus formalism. The (α,n) and (p,n) excitation functions both rise to a maximum of about 130 mb at 15 MeV and fall to around 10 mb at 38 MeV. The calculated cross sections according to the compound-nucleus mechanism are in reasonable agreement with the experimental results except at the high-energy end—where, nevertheless, both the shapes and the magnitudes of the two excitation functions are the same.

I. INTRODUCTION

THERE have been a few studies of the total cross sections for radiative capture by complex nuclei of various charged particles with energies ranging from about 5 up to about 40 MeV.[1–8] In these investigations it was found that the observed cross sections for the radiative capture of protons were usually larger than those expected from a calculation in which the photon was taken to be emitted subsequent to compound-nucleus formation,[1] whereas this model was moderately successful in the interpretation of radiative capture of alpha particles and deuterons.[2,4–7] This discrepancy leads to the suggestion that there is an important contribution of a direct proton radiative capture.[9–12]

The previous experimental investigations have been carried out on a variety of targets and could only be intercompared by means of approximate calculations based upon some model for the mechanism of the reaction. In this situation it would clearly be advantageous to investigate a system in which the same radiative-capture product is made in at least two different ways. Accordingly, we have measured the excitation functions for the $Ce^{142}(p,\gamma)Pr^{143}$ and the $La^{139}(\alpha,\gamma)Pr^{143}$ reactions in the bombarding-energy interval of about 10 to 40 MeV.[8] As will be seen below, the maximum in the (p,γ) excitation function is an order of magnitude larger than that for the (α,γ) reaction; an observation that gives direct support to a process operative in proton radiative capture that is not significant in alpha-particle radiative capture.

The $Ce^{142}(p,n)Pr^{142}$ and $La^{139}(\alpha,n)Pr^{142}$ excitation functions were also measured so as to supply some information about the total-reaction cross section in the low-energy region.

II. EXPERIMENTAL

A. Target Preparation

The lanthanum and cerium targets were prepared by the electrophoretic deposition of rare-earth oxides on a 1-mil aluminum foil.[13] The average thickness of the deposits was a few mg/cm^2; the targets for the proton bombardments were squares of 1 in. by 1 in. For alpha bombardment, targets of two different shapes and sizes were used: squares 1 in. by 1 in. and rectangular targets 2 in. by 1 in. Each deposit was cut in half and glued together face to face so as to give greater target thickness. The aluminum backing thus served to catch the forward and backward recoiling particles.

B. Target Irradiations

The stacked-foil method was used for the simultaneous irradiation of from 3–7 targets in each bombardment. Aluminum foils placed in the stack served to degrade the beam, and copper foils were placed in the

* Work supported in part by the U. S. Atomic Energy Commission.
† Submitted in partial fulfillment of requirements for the Ph.D. degree.
‡ National Science Foundation Senior Postdoctoral Fellow.
[1] B. L. Cohen, Phys. Rev. **100**, 206 (1955).
[2] H. Morinaga, Phys. Rev. **101**, 100 (1956).
[3] C. G. André *et al.*, Phys. Rev. **101**, 645 (1956).
[4] J. H. Carver and G. A. Jones, Nucl. Phys. **11**, 400 (1959).
[5] J. H. Carver and G. A. Jones, Nucl. Phys. **24**, 607 (1961).
[6] F. K. McGowan, P. H. Stelson, and W. G. Smith, Phys. Rev. **133**, B907 (1964).
[7] J. Ball and A. W. Fairhall, Phys. Rev. **114**, 305 (1959).
[8] Daly and Shaw have recently reported their measurement of the $Ce^{142}(p,\gamma)Pr^{143}$ excitation function [P. J. Daly and P. F. D. Shaw, Nucl. Phys. **56**, 322 (1964)]. The results of the two sets of measurements are in excellent agreement, except perhaps at higher energies, where the cross sections reported here tend to be somewhat smaller.
[9] F. Beck, Nucl. Phys. **9**, 140 (1959).
[10] A. M. Lane and J. E. Lynn, Nucl. Phys. **11**, 625 (1960); **11**, 646 (1960); C. F. Clement, A. M. Lane, and J. R. Rook, *ibid.* **66**, 273 (1965).
[11] R. F. Christy and I. Duck, Nucl. Phys. **24**, 89 (1961).
[12] G. E. Brown, Nucl. Phys. **57**, 339 (1964).
[13] S. Bjørnholm, Ph. Dam, H. Nordby, and N. O. Poulsen, Nucl. Instr. Methods **5**, 196 (1959).

stack as a monitor of the beam energy and current by means of the known excitation functions for the production of Zn^{65} by alpha particles and by protons with copper. The energy of the proton beam at various positions in the stack was estimated from the range-energy tables of Sternheimer[14] for protons in copper and aluminum. The La_2O_3 and CeO_2 range-energy curves were calculated by interpolating the experimental results of Bichsel *et al.*[15] according to Friedlander, Kennedy, and Miller.[16] The energy of the alpha beam at various points in the stack was estimated from the range-energy data of Northcliffe[17] for alpha particles in copper and aluminum.

1. *Irradiation with Alpha Particles*

The irradiations were performed in the external 40-MeV alpha-particle beam of the Brookhaven 60-in. cyclotron. The absolute beam intensity was measured to within 5% with a Faraday cup[18] which was calibrated before and after each bombardment. In the early bombardments the beam was collimated to a $\frac{1}{4}$-in. diam and the intensity was 0.5–1 μA. Since higher beam currents were needed for measuring the (α,γ) reaction, this collimator was removed in later bombardments and a rectangular beam with dimensions of $\frac{1}{3}$ in. by 1 in. and a current of 3–10 μA was used instead. The production of Zn^{65} in the copper monitor foils through the reactions $Cu^{63}(\alpha,pn)Zn^{65}$ and $Cu^{65}(\alpha,p3n)$-Zn^{65} was used as a measure of the energy of the beam at various points in the stack as well as the effective beam current through the target. These monitor reactions were calibrated in a stacked-foil bombardment of $\frac{1}{4}$ mil copper foils with 40-MeV alphas, whose energy was determined by range measurements.

2. *Irradiations with Protons*

Protons of up to 12.5 MeV with beam intensities of 0.05–0.250 μA were obtained from the Columbia University 36-in. cyclotron. The beam was collimated to a circle of $\frac{1}{4}$-in. diam, and its intensity was measured with a Faraday cup. The energy of the beam at various points in the stack was measured through the excitation function of the $Cu^{65}(p,n)Zn^{65}$ reaction, which in turn was determined using the 10-MeV protons of the Brookhaven cyclotron. The results agreed with the measurements of Wing and Huizenga[19] and of Howe.[20]

For the lower energy region of the excitation function, the 5-MeV protons of the Columbia Van de Graaff accelerator were used; the higher energy region was investigated with the 88-in. cyclotron at Berkeley.

C. Chemical Procedures

The standard chemical procedures used to effect the separation of reaction products from the target material, determination of target thickness, and determination of the efficiency of separation of reaction products are described in an appendix.

D. Disintegration-Rate Determination

The disintegration rates of the Pr samples were determined through their beta and gamma radiations.

The beta particles were detected with beta-proportional counters which were calibrated with standards of P^{32} (a 1.71-MeV beta emitter) and Cl^{36} (a 0.714-MeV beta emitter); both standards were provided by the National Bureau of Standards. Self-absorption and back-scattering effects were found to be negligible for the samples used. The uncertainty in the efficiency of the detector was estimated to be 5%. Two separate calibrations were made with each standard and found to agree to within 4%.

The gamma rays were counted in a 3 in. by 3 in. NaI(Tl) crystal in conjunction with a 400-channel TMC pulse-height analyzer. The crystal was calibrated with standards of various energies for photopeak efficiencies. The uncertainty in a given photopeak efficiency is less than 10%.

The Pr samples were checked first for impurities on the 400-channel TMC pulse-height analyzer with the 3 in. by 3 in. NaI(Tl) crystal. Since Pr^{143} is a pure beta emitter and Pr^{142} emits, in addition to a beta, a 1.57-MeV gamma ray which occurs to a 4% abundance, only this gamma ray and the usual bremsstrahlung should be present. The separations were repeated if gamma rays from Ce or La activities were detected, although in several samples these impurities were not entirely eliminated.

The Pr^{142} disintegration rate was measured through its 0.58- and 2.15-MeV beta rays[21] in the beta-proportional counter as well as through its 1.57-MeV gamma ray in the NaI(Tl) crystal. The two results agreed to 5–7%. The observed half-life checked with the 19.3 h that has been reported.

The disintegration rate of the Pr^{143} was determined by means of its 0.93 beta with the half-life taken to be 13.8 days.[21] Each sample was counted for about four months. Occassionally, in samples with very small amounts of Pr^{143}, the 32.5-day half-life of Ce^{141} would be present in the decay curve. Under these circumstances the decay curves were analyzed both graphically and

[14] R. M. Sternheimer, Phys. Rev. **115**, 137 (1959).
[15] H. Bichsel, R. Mozley, and W. Aron, Phys. Rev. **105**, 1788 (1957).
[16] G. Friedlander, J. Kennedy, and J. M. Miller, *Nuclear and Radiochemistry* (John Wiley & Sons, Inc., New York, 1964), 2nd ed., p. 98, Eq. (4–9).
[17] L. C. Northcliffe, Phys. Rev. **120**, 1744 (1960).
[18] S. Amiel and N. T. Porile, Rev. Sci. Instr. **29**, 1112 (1958).
[19] J. Wing and J. R. Huizenga, Phys. Rev. **128**, 280 (1962).
[20] H. A. Howe, Phys. Rev. **109**, 2083 (1958).
[21] *Nuclear Data Sheets* compiled by K. Way *et al.* (Printing and Publishing Office, National Academy of Sciences—National Research Council, Washington 25, D. C.), NRC 61-4-40.

TABLE I. Experimental cross sections for protons and cerium-142.

Kinetic energy (MeV)	Excitation energy (MeV)	Bombardment	$\sigma(p,n)$ (mb)	$\sigma(p,\gamma)$ (μb)
3.0	9.0	1	0.0001	
3.8	9.8	2	0.163	
4.0	10.1	1	0.7	
5.8	11.9	6	10.8	
6.1	12.1	3	3.5	18
6.3	12.3	5	5.0	10
6.9	12.9	6	48.8	37.5
7.1	13.2	3	38.0	55
7.2	13.2	4	80.0	42
7.3	13.3	5	32.6	36
8.0	14.0	6	113	95
8.2	14.2	3	125	
8.5	14.5	5	90	121
8.9	14.9	3	100	134
9.1	15.1	6	131	224
9.1	15.1	4	125	220
9.5	15.5	5	109	161
9.7	15.7	3		270
10.0	16.0	4	64	282
10.0	16.0	6	91	308
10.5	16.4	5	108	364
10.7	16.7	6	72.3	406
10.8	16.7	4	48.0	464
11.1	17.1	7	61.0	519
11.7	17.1	7	38.0	376
12.0	18.0	5	48.0	536
12.8	18.8	7	59.0	650
13.8	19.8	7	44.7	616
16.0	22.0	7	31.6	540
18.0	23.9	7	27.0	404
19.9	25.8	7	24.0	322
23.2	29.1	8	26.0	240
26.7	32.6	8	20.0	169
29.9	35.8	8	11.0	80

with a least-squares computer program.[22] The two methods agreed to within 15%.

The Zn^{65} activity produced in the monitor reaction with copper was detected and assayed through its 1.12-MeV gamma ray.

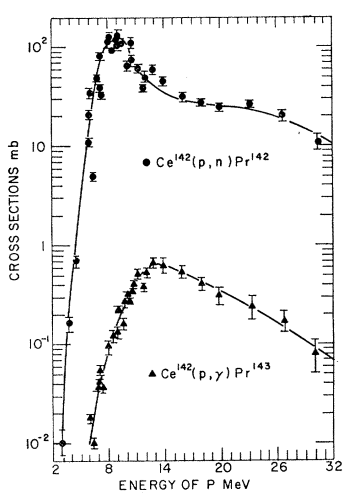

FIG. 1. Cross sections for $Ce^{142}(p,n)Pr^{142}$ and $Ce^{142}(p,\gamma)Pr^{143}$ reactions in mb versus laboratory energy of proton.

[22] J. B. Cumming, Brookhaven National Laboratory Report No. BNL 6470, 1962 (unpublished).

TABLE II. Experimental cross sections for alphas and lanthanum-139.

Kinetic energy (MeV)	Excitation energy (MeV)	Bombardment	$\sigma(\alpha,n)$ (mb)	$\sigma(\alpha,\gamma)$ (μb)
10.1	8.0	5	0.319	
12.3	10.1	8	2.3	4.2
13.2	10.9	3	2.8	28.3
13.2	11.0	7	25	24.6
13.4	11.1	3	65	47.1
16.3	14.0	4	85	47.0
16.9	14.6	6	105	61.0
17.6	15.2	2	125	82.8
18.0	15.7	3	98	62.8
19.1	16.7	7	86	64.8
20.1	17.7	1	81	65.4
20.3	17.8	8	80	65.0
21.0	18.6	2	44	58.3
21.1	18.7	6	53	50.0
21.4	19.0	5	97	73.3
21.8	19.4	3	41.4	58.5
23.5	21.0	8	32.0	36.0
24.5	21.9	4	30.0	33.9
26.0	23.4	6	43.6	33.8
27.1	24.5	2	23.1	18.4
27.9	25.3	3	21.9	14.6
29.0	26.3	7	21.2	13.3
32.5	29.7	8	19.0	11.0
34.1	31.3	5	15.3	
35.2	32.3	7	12.1	
36.1	33.3	4	11.3	
36.9	34.1	3	11.9	
38.2	35.3	2	7.9	
39.0	36.1	7	14.2	
39.6	36.6	6	7.3	

E. Experimental Results and Sources of Error

1. Experimental Results

Cross sections from the various irradiations are listed in Tables I and II and shown in Figs. 1 and 2. The cross sections are calculated from the experimentally measured quantities in the usual manner according to the formula

$$\sigma = D/in(1-e^{-\lambda t}), \tag{1}$$

where D is the disintegration rate (in min^{-1}) of a

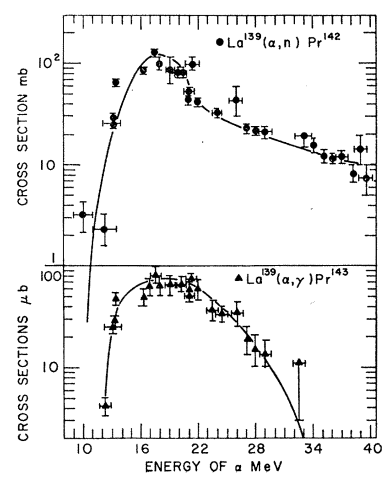

FIG. 2. Cross section for $La^{139}(\alpha,n)$-Pr^{142} and $La^{139}(\alpha,\gamma)$-Pr^{143} reactions in mb and μb, respectively, versus laboratory energy of alpha particle.

product nuclide in the target at the end of the bombardment, n is the number of target atoms per cm^2, i is the beam current in protons per minute, λ is the decay constant in min^{-1}, t is the length of bombardment in minutes; σ then is given in cm^2 per atom.

2. *Sources of Error*

There are two kinds of errors that must be considered: those that affect the magnitude of the cross section and those that affect the energy dependence of the cross section.

(*a*) *Proton bombardments.* The total amount of target material in each run was determined by chemical analysis; the area of the target was determined by weighing an aluminum foil of the same area and of known thickness. The error in the procedure, and thus in the quantity n, is estimated to be about 5%. In a few experiments the targets were cut into many pieces and the thickness of each piece was determined in the manner that was just described. The maximum fluctuation in surface density was found to be 5%.

The proton beam at the Columbia cyclotron was checked for contamination from deuterons or secondary neutrons which could interfere with the determination of the $Ce^{142}(p,\gamma)Pr^{143}$ cross section through the following nuclear reactions:

(a) $Ce^{142}(n,\gamma)Ce^{143}$ $Ce^{143} \rightarrow Pr^{143}+\beta^-$,
(b) $Ce^{142}(d,p)Ce^{143}$ $Ce^{143} \rightarrow Pr^{143}+\beta^-$,
(c) $Ce^{142}(d,n)Pr^{143}$.

If Ce^{143} was produced by reaction (a), it should be more easily detected as the decay product Pr^{143} at the low-energy end of the stack where the amount (if any) of Pr^{143} produced through the (p,γ) reaction is much smaller. It could also be detected as Ce^{143} before decaying to Pr^{143}. Accordingly, the Ce fractions from the low-energy samples were checked in a 400-channel pulse-height analyzer for the existence of the 0.29- and 0.66-MeV Ce^{143} gamma rays; they were not observed. Moreover, there was no detectable Pr^{143} activity in the Pr samples from the low-energy targets. From these measurements, an upper limit of 10 μb could be placed on the contribution of reaction (a) to the apparent (p,γ) cross section.

Since there was no detectable neutron contamination, production of Ce^{143} through reaction (b) was also used as a deuteron monitor in the higher energy targets. Again, the characteristic gamma rays of Ce^{143} were not observed and the contribution from reactions (b) and (c) to the measured cross sections could be taken as negligible.

The contamination by neutrons was not directly checked in the bombardments at the Berkeley cyclotron. It was assumed that since the cross sections at 10–12 MeV were consistent with these measurements at Columbia, there was no detectable (n,γ) contribution in the bombardments at Berkeley.

There were no contaminating activities present in the Pr samples in the measurement of the (p,n) cross sections at low energies. Individual points on the decay curves had a standard deviation of 1% and there was a standard deviation of about 2% in the activity extrapolated back to zero time. At higher energies, 20–30 MeV, there is interference from incomplete separation of the 40.2-h La^{140} produced by the $Ce^{142}(p,2pn)La^{140}$ reaction. The resulting composite decay curve of the 19.3-h Pr^{142} and 40.2-h La^{140} was easily resolved.

The largest error occurs in the determination of the Pr^{143} counting rate. The difficulty comes from the contamination of the Pr^{143} fraction with Ce^{141} formed in the $Ce^{142}(p,pn)Ce^{141}$ reaction. It was not always possible to achieve adequate chemical separation of the two, as the counting rate of Ce^{141} could be as much as 10^4 greater than that of Pr^{143}. The uncertainty in the analysis of the resulting complex decay curve is reflected in an error of about 5% in the (p,γ) cross section at low energies, rising to as much as 30% at energies above 23 MeV.

The beam current was measured both by use of a Faraday cup and through the $Cu^{65}(p,n)Zn^{65}$ monitor reaction. The estimated error in these measurements of of the beam current was about 10% at the Columbia Van de Graaff and about 5% at the Columbia cyclotron.

The estimated error in the measurement of the beta counter efficiencies by means of standard samples was 5%. Similarly the estimated error in the efficiencies of the 3-in. by 3-in. NaI(Tl) crystal was 10%.

Estimation of the error in the cross sections that result from the foregoing effects are summarized in Table III.

The errors in the assignment of the energy value to the cross section result from: (1) energy spread in the beam and (2) the estimation of its average value at various points in the stack of targets.

The energy spread is $\simeq$100 keV for the Columbia Van de Graaff, $\simeq$250 keV for the Columbia cyclotron,

TABLE III. Estimated cumulative errors in the experimental cross sections.

Incident particles	Reaction	Error (%)
Protons		
Van de Graaff	(p,n)	±13.0
Cyclotron-Columbia	(p,n)	±10.0
	(p,γ)	±11.0
Cyclotron-Berkeley		
12–20 MeV	(p,n)	±13.0
20–30 MeV	(p,n)	±17.0
12–23 MeV	(p,γ)	±14.0
23–30 MeV	(p,γ)	±33.0
Alphas		
10–30 MeV	(α,n)	±13.0
32–40 MeV	(α,n)	±17.0
10–32 MeV	(α,γ)	±14.0
32–40 MeV	(α,γ)	±33.0

≃300 keV for the Berkeley cyclotron. At low energies the spread is about twice that given above in each bombardment because the lower energy protons of the beam lose more energy in the stack than do those at higher energy. Variations in the thickness of the targets or variation in the thickness of the other foils in the stack represent a negligible source of energy spread. Beam straggling effects are negligible, since in no stack was the beam degraded by more than 10 MeV.

(*b*) *Alpha bombardments*. Errors in the target thickness and uniformity, chemical yields, and efficiencies of counters were the same as for incident protons.

The 40.2-h La^{140} which was formed in the $La^{139}(n,\gamma)$-La^{140}, $La^{139}(d,p)La^{140}$, and $La^{139}(\alpha,2pn)La^{140}$ reactions could interfere with the determination of the 19.3-h Pr^{142} if the chemical separation was not sufficiently complete. When this occurred, the complex decay curve (19.3-day Pr^{142} and 40.2-h La^{140}) was analyzed both graphically and by a least-squares program.

In the measurement of the (α,γ) cross section the largest error was caused by the occasional contamination of the Pr^{143} fraction with Ce^{141} formed in the La^{139}-$(\alpha,pn)Ce^{141}$ reaction (with a 14.7-MeV threshold). The resulting complex decay curve was analyzed, as was that for incident protons, with the same uncertainty in the analysis.

A significant amount of La in the Pr could affect the chemical yield determination, since the analytical procedure that was employed did not differentiate between Pr and La. To check on this source of error, the 1.60- and 0.49-MeV gamma rays from the La^{140} in the La fraction of the rare-earth separation were counted and compared with the same activity, if any, that was detected in the Pr fraction. From this comparison it was found that the error in the chemical yield determination, resulting from La contamination of the Pr fraction, was never larger than 10%.

The error in the measurement of the beam current by integration of the charge collected on the Faraday cup is estimated to be about 5%.

In a few alpha bombardments there was some leakage of target cooling water into the target stack. This caused the loss of some target material and introduced an error of about 30% into those targets that were salvageable.

The errors in the assignment of the energy at each point in the stack of foils are 200 keV in the beam of small diameter and 500 keV in the beam of large diameter. This increased to about twice that amount at the low-energy end of the stack, just as for protons.

The cumulative errors in the cross-section measurements are again summarized in Table III.

III. DISCUSSION

The two processes that were examined in this investigation of the de-excitation of the Pr^{143} compound system formed by alpha-particle bombardments of

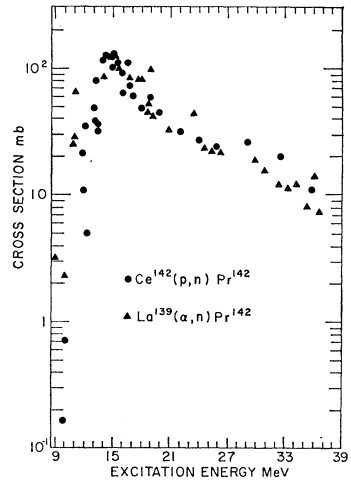

FIG. 3. Cross sections for $La^{139}(\alpha,n)Pr^{142}$ and $Ce^{142}(p,n)Pr^{142}$ reactions in mb versus excitation energy of the compound nucleus.

La^{139} and proton bombardments of Ce^{142} are neutron emission and photon emission.

The dependence of the (p,n) and (α,n) excitation functions on bombarding energy are shown in Figs. 1 and 2, and upon excitation energy of the compound system in Fig. 3. The maxima in both curves occur at nearly the same excitation energy of approximately 15 MeV and at the same magnitude of about 125 mb. Both curves exhibit high-energy tails of similar shape and magnitude. It is found that the neutron emission, which will be discussed in Sec. III A, can be described, in the main, simply by means of conventional evaporation theory.

As was anticipated, the gamma-ray emission presents a more complex situation, as is evident from the (p,γ) and (α,γ) excitation functions shown in Figs. 1 and 2 and as a function of excitation energy in Fig. 4. Contrary to those for the (p,n) and (α,n) reactions, there is an order-of-magnitude difference in their maxima as well as a difference in their shape, particularly at high energies. We note that the (p,γ) excitation function reaches a maximum at around 19 MeV, as compared to

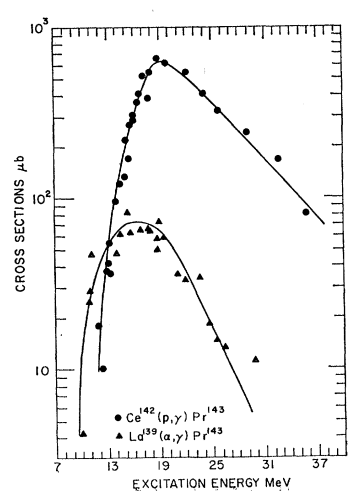

FIG. 4. Cross sections for $La^{139}(\alpha,\gamma)Pr^{143}$ and $Ce^{142}(p,\gamma)Pr^{143}$ reactions in mb versus excitation energy of the compound nucleus.

around 17 MeV for the (α,γ) reaction, and it decreases more gradually than does the (α,γ) at high energies. Since both reactions proceed through the same compound system Pr^{143}, it is obvious that another mechanism contributes to the (p,γ) excitation function. Therefore, any attempt to analyze the excitation function for a (p,γ) reaction must contain a direct as well as a compound-nucleus contribution. It is obvious, though, that the noncompound process will have to include the giant dipole resonance so as to preserve the peak in the excitation function which, while not as sharp as for the (α,γ) reaction, clearly exists. These points will be considered in Sec. III B.

A. Neutron-Emission Reactions

A reaction proceeding by the compound-nucleus mechanism can be represented by

$$a+A\rightarrow C^*\rightarrow b+B\,, \tag{2}$$

where C^* is the compound nucleus that is formed. The cross section, if the effects caused by the angular momentum distribution of the compound nuclei are neglected, may be written as[23]:

$$\sigma_{A\rightarrow C\rightarrow B}=\sigma_{A\rightarrow C}W_B\,, \tag{3}$$

where $\sigma_{A\rightarrow C}$ is the cross section for the formation of the compound nucleus C^* and W_B is the probability that the compound nucleus C^* decays by emission of a particle (or gamma ray) b leaving a residual nucleus B. The quantity W_B may be expressed as

$$W_B=\Gamma_{Bb}/\Gamma\,, \tag{4}$$

where Γ_{Bb} is the partial width of the level for emission of particle b leading to a residual nucleus B that is particle stable and Γ is the total emission width of the level.

Equation (3) was used for the estimation of the excitation functions of the $Ce^{142}(p,n)Pr^{142}$ and La^{139}-$(\alpha,n)Pr^{142}$ reactions. In the calculation, W_B was computed by the method of Dostrovsky, Fraenkel, and Friedlander[24] using a radius parameter of 1.5 F, a level-density parameter of $A/20$, where A is the mass number of the nucleus in question, and ground-state-displacement correction for shell and pairing effects from Cameron.[25] The total width in Eq. (4) included contributions from the emission of n, p, α, and any combination thereof. The cross sections for compound-nucleus formation were computed by the ABACUS II program of Auerbach[26] and are compared with other calculations[27,28] in Figs. 5 and 6. The results of these calculations are compared with those from experiment in Fig. 5 for the (p,n) excitation function and in Fig. 6 for the (α,n) excitation function. There is satisfactory agreement between the theoretical and experimental results up to a few MeV beyond the maxima in the excitation functions, at which point the usual high-energy tail appears, which is, as usual, not reproduced by the calculation of the type used here. In Fig. 3 it was seen that these high-energy tails on the two excitation functions are, within experimental error, *identical* to each other. This observation makes it difficult to accept either of the two current explanations of their existence: angular momentum effects and direct interaction. Since La^{139} has a ground state spin of $\frac{5}{2}$ as compared to that of 0 for Ce^{142} and since the alpha particle carries in, on the average, more orbital angular momentum than does a proton in the range of kinetic energies of importance

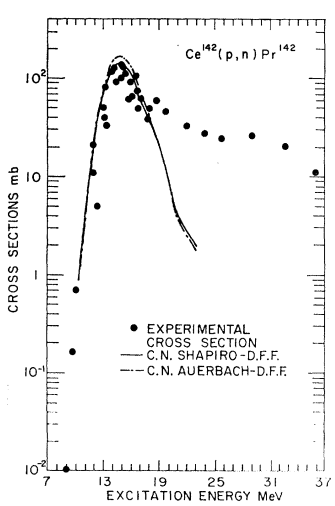

FIG. 5. Comparison between calculated and experimental excitation functions for the Ce^{142}-$(p,n)Pr^{142}$ reaction. Solid curve is based upon reaction cross section from Shapiro (Ref. 28); dash-dot curve is based upon reaction cross section from optical model as calculated with ABACUS-2 of Auerbach (Ref. 26).

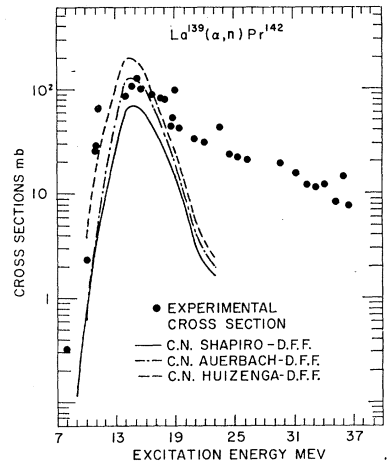

FIG. 6. Comparison between calculated and experimental excitation function for the La^{139}-$(\alpha,n)Pr^{142}$ reaction. Reaction cross sections used are: solid curve from Shapiro (Ref. 28), dashed curve from Huizenga and Igo (Ref. 27), and dash-dot curve from ABACUS-2 program of Auerbach (Ref. 26).

[23] Reference 16, Chap. 10.

[24] I. Dostrovsky, Z. Fraenkel, and G. Friedlander, Phys. Rev. **116**, 683 (1960).

[25] A. G. W. Cameron, Can. J. Phys. **36**, 1040 (1958).

[26] E. H. Auerbach, Brookhaven National Laboratory Report No. BNL 6562, 1962 (unpublished). The depths of the real and imaginary potentials were taken to be $50-0.42E$ and $4.5+0.39E$, respectively, where E is the bombarding energy and energies are in MeV. The usual Saxon-Woods form factor was used with real and imaginary diffuseness parameters of 0.65 and 0.98 F, respectively. The half-density distances were taken to be 6.55F for protons and 7.25F for alpha particles.

[27] J. R. Huizenga and G. J. Igo, Argonne National Laboratory Report No. ANL 6373, 1961 (unpublished).

[28] M. M. Shapiro, Phys. Rev. **90**, 171 (1953).

here, angular-momentum effects would make the tail on the (α,n) reaction higher than that for the (p,n) reaction. The possible direct interactions would presumably be either a stripping of the alpha particle or a direct ejection of a neutron by the alpha particle in the (α,n) reaction and a direct ejection of a neutron by the proton in the (p,n) reaction. It would be remarkable indeed if both of these rather different direct processes had the same values and energy dependence of their cross sections.

B. Gamma-Ray Emission Reactions

1. Calculation of Cross Sections for Gamma-Ray Emission by the Compound-Nucleus Process

The cross section for capture of projectile a by the target A with subsequent emission of a photon through the compound-nucleus mechanism is given by Eq. (3). In this instance, the particle b is a photon, and so W_γ is the probability that the compound system C^* decays by emission of a gamma ray, leaving C as the residual nucleus;

$$W_\gamma = \Gamma_\gamma/\Gamma, \tag{5}$$

where Γ_γ is now the partial width of the level for emission of a gamma ray. The quantity Γ_γ may be written as

$$\Gamma_\gamma = \hbar \int_{U_C - B_n}^{U_C} I(\epsilon_\gamma) d\epsilon_\gamma, \tag{6}$$

where $I(\epsilon_\gamma)$ is the probability per unit time that the compound nucleus of excitation energy U_C emits a gamma ray with energy between ϵ_γ and $\epsilon_\gamma d\epsilon_\gamma$. The lower limit of integration is taken as $U_C - B_n$, where B_n is the neutron binding energy, so that the residual nucleus C will be stable against particle emission. Actually the binding energy of the proton is about 1.2 MeV less than that of the neutron in Pr^{143}, but the Coulomb barrier will cause any final state below the neutron threshold to decay mainly by photon emission.

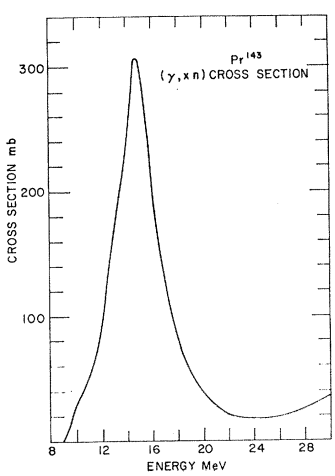

FIG. 7. Energy dependence of photoneutron cross section of Pr^{141} from Ref. 29. It is assumed to be the same for Pr^{143}.

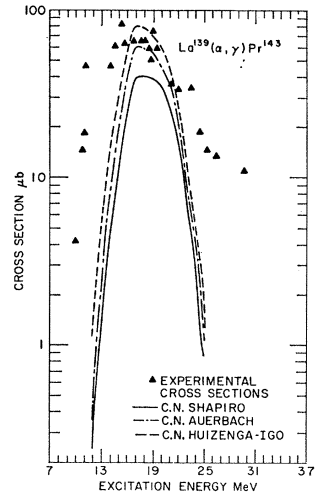

FIG. 8. Calculated and experimental excitation functions for the La^{139}-$(\alpha,\gamma)Pr^{143}$ reaction. See Fig. 6 for significance of the calculated curves.

The expression for $I(\epsilon_\gamma)$ is

$$I(\epsilon_\gamma)d\epsilon_\gamma = \frac{\sigma_\gamma(\epsilon_\gamma)\epsilon_\gamma^2 \rho(U_C - \epsilon_\gamma) d\epsilon_\gamma}{c^2 \pi^2 \hbar^3 \rho(U_C)}, \tag{7}$$

where c is the velocity of light, $\sigma_\gamma(\epsilon_\gamma)$ is the cross section for the absorption of gamma rays of energy ϵ_γ by nuclei C at an excitation energy of $U_C - \epsilon_\gamma$, and $\rho(U)$ is the level density of the nucleus C at energy U and is taken to have the form given in Ref. 24:

$$\rho(U) \propto e^{2a^{1/2}(U-\delta)^{1/2}}, \tag{8}$$

where a and δ are parameters that characterize the nucleus under consideration. We shall approximate the cross section for capture of the gamma rays by the nucleus C in an excited state by the ground-state cross section and take for this the experimental measurement of Rice, Bolen, and Whitehead[29] for the photoneutron cross section of Pr (Fig. 7).

The expression for Γ_γ was then calculated by numerical integration of Eq. (7), and $\Gamma\gamma/\Gamma$ and $\sigma_{A\to C}$ were then computed. It may be seen from Fig. 8 that the calculated and experimental (α,γ) excitation functions peak at about the same excitation energy of 17–18 MeV and have the same maximum cross section of about 70 μb. The divergence between the calculated and measured cross sections both above and particularly below the maximum may be partly explained by an underestimation of $\sigma_\gamma(\epsilon_\gamma)$. In this calculation $\sigma_\gamma(\epsilon_\gamma)$ was approximated by the photoneutron cross section, which is expected to be essentially equal to the absorption cross section at medium energies, but not at low or high energies. For ϵ_γ below the binding energy of a neutron (7.22 MeV for Pr^{143}) where the photoneutron cross section vanishes, $\sigma_\gamma(\epsilon_\gamma)$ does not necessarily vanish and is probably equal to the (γ,γ') inelastic-scattering cross section. This effect was not included

[29] L. B. Rice, L. N. Bolen, and W. D. Whitehead, Phys. Rev. 134, B557 (1964).

because of the lack of experimental or theoretical estimates of the (γ,γ') cross section. At high energies, the photoneutron cross section is expected to be only a lower limit to $\sigma_\gamma(\epsilon_\gamma)$ because of competition from, for example, (γ,p) and (γ,α) reactions. This competition, though, is probably not too important, and the neglect in the present calculation of the emission of two or more photons in cascade[10] is likely to be a more important effect. On the whole, though, the agreement between calculated and experimental values is satisfactory.

Since both the (α,γ) and (p,γ) reactions that are studied here proceed through the same compound system Pr^{143}, and since the capture cross section of alphas by La^{139} and protons by Ce^{142} to give compound systems at the same excitation energies happen to be not very different, the compound-nucleus contribution to the (p,γ) excitation functions is essentially the same as that for the (α,γ) reaction. From Fig. 4, then, it may be seen that the compound-nucleus mechanism can contribute at most 10% of the observed (p,γ) cross section; the remainder must be some sort of nonstatistical process.

2. *Direct and Semidirect (Collective) Radiative Proton Capture*

The radiative capture of protons by nonstatistical processes has been discussed in several papers.[9–12] The first process that has been considered is the direct dipole radiative transition of the proton from an initial independent-particle state in the continuum to one that is bound.[10] It is clear, though, from Fig. 4, that it is not likely that this process is the dominant one because there is no reason that independent single-particle transitions would give a rather well-defined maximum in the excitation function in the region of the giant photonuclear resonance. That this is indeed the situation is illustrated in Fig. 9, where a calculation by Daly, Rook, and Hodgson[30] of the cross section for the direct radiative capture of protons (the dashed line) is compared with the experimental results of the present investigation and of Daly *et al.*[8]

The consideration of higher order terms in the amplitude for proton capture[12] entails the dipole state and, as is seen in Fig. 9 from the detailed calculation of Clement, Lane, and Rook,[31] gives considerably better agreement with the experimental results. This latter contribution to the radiative capture has been called either "semidirect" or "collective" capture.

There are, then, three significant contributions to the cross section for the $Ce^{142}(p,\gamma)Pr^{143}$ reaction: direct capture, indirect capture, and compound-nucleus formation. The last contribution may be estimated from the results given in Tables I and II if it is assumed that

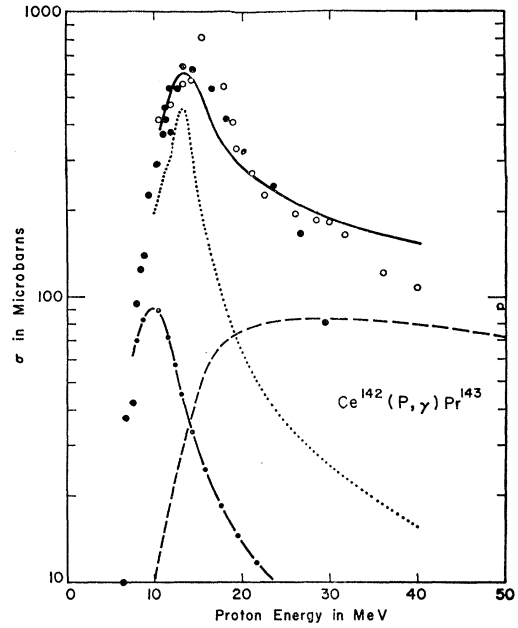

FIG. 9. Comparison between calculated and experimental values of the laboratory energy dependence of the $Ce^{142}(p,\gamma)Pr^{143}$ reaction. The experimental points are: open circles, from Daly and Shaw (Ref. 8) and closed circles, from present experiment. The calculated curves are: dash-dot, compound-nucleus contribution based upon measured cross section for (α,γ), (α,n), and (p,n) reactions; dashed, direct capture from Daly *et al.* (Ref. 30); dotted, collective capture from Clement *et al.* (Ref. 31); straight-line, sum of all three contributions assuming that the amplitudes for direct and collective capture add.

the independence hypothesis for compound-nucleus reactions holds for the (α,n), (α,γ), and (p,n) reactions as well as for that part of the (p,γ) reaction that proceeds through the formation of a compound nucleus. Under this assumption, at a given excitation energy of the compound nucleus and ignoring any effects imposed by angular momentum considerations:

$$\frac{\sigma(\alpha,\gamma)}{\sigma(\alpha,n)}=\frac{\sigma'(p,\gamma)}{\sigma(p,n)},$$

where $\sigma'(p,\gamma)$ is the compound-nucleus contribution to the cross section of the (p,γ) reaction. The contribution to the excitation function that is calculated in this manner is shown as the dash-dot curve in Fig. 9. The total (p,γ) cross section will depend on the relative phases of the amplitudes for the direct and semidirect capture. If it is assumed that they are in phase, then the total calculated cross section is given by the solid curve in Fig. 9.

IV. CONCLUSIONS

(1) The $La^{139}(\alpha,\gamma)Pr^{143}$ reaction seems to proceed mainly through a compound-nucleus mechanism. An excitation function that is calculated on the basis of this mechanism gives reasonable agreement with the experimental results.

[30] P. J. Daly, J. R. Rook, and P. E. Hodgson, Nucl. Phys. **56**, 331 (1964).
[31] C. F. Clement, A. M. Lane, and J. R. Rook, Nucl. Phys. **66**, 293 (1965).

(2) The $Ce^{142}(p,\gamma)Pr^{143}$ reaction, whose peak cross section is about an order of magnitude larger than that for the $La^{139}(\alpha,\gamma)Pr^{143}$ cross section, seems to proceed mainly through a mechanism other than compound nucleus, presumably direct and semidirect proton capture.

(3) The $La^{139}(\alpha,n)Pr^{142}$ and $Ce^{142}(p,n)Pr^{142}$ excitation functions are in good agreement with those expected for a compound-nucleus reaction except for a high-energy tail. Since the magnitude and the shape of the tail is much the same for both reactions, it is difficult to ascribe it to a simple direct process.

ACKNOWLEDGMENTS

We wish to express our gratitude to Dr. C. P. Baker and the crew of the Brookhaven 60-in. cyclotron for performing irradiations, Dr. M. Slavin for spectrographic analyses, and Dr. R. W. Stoenner for chemical analyses. We wish also to thank Dr. L. Feldman and the staff of the Columbia 36-in. cyclotron, as well as Professor L. Lidofsky, Dr. A. Sayres, and the staff of the Columbia Van de Graaff. We are especially indebted to H. A. Grunder and Mrs. R. M. Larimer for arranging so efficiently for the irradiations at the Berkeley 88-in. cyclotron and operating crew for performing them.

The support of the U. S. Atomic Energy Commission is gratefully acknowledged.

APPENDIX

1. Lanthanum Targets

After irradiation, the La_2O_3 targets were cut around the region of beam impact. The area of this region was measured by weighing a piece of aluminum foil of the same area and of known surface density. These cut-out portions of target were then dissolved in concentrated HCl and made up to volume in a volumetric flask. An aliquot of this solution was put aside for the determination of La_2O_3 content. Sodium, praseodymium, and cerium carriers were added to the remaining solution and the rare earths were precipitated with concentrated HF after the pH was adjusted to 5.0 with NH_4OH so as to prevent the precipitation of aluminum. The rare-earth fluorides were then dissolved in $6M$ HNO_3 saturated with H_3BO_3, and the hydroxides were precipitated with NH_4OH. After dissolution of the hydroxides in $6M$ HNO_3, Ce^{3+} was oxidized to Ce^{4+} with $(NH_4)_2S_2O_8$ with $AgNO_3$ added as an indicator. The Ce^{4+} was then extracted into a mixture of 30% tributylphosphate and 70% CCl_4, leaving praseodymium and lanthanum in the aqueous phase. The cerium was back extracted from the organic phase into $1M$ HCl containing solid $NaHSO_3$ and was precipitated as $Ce_2(C_2O_4)_3$ with oxalic acid at pH 2.3. The precipitate was filtered, dried, and placed on an aluminum card for counting.

The excess oxidizing agent in the aqueous phase was reduced with H_2O_2 and then NH_4OH was added to precipitate the $La(OH)_3$ and $Pr(OH)_3$. The precipitates were dissolved in $1M$ HCl and the solution was passed through a Dowex 50W-X8 (200–400 mesh) cation exchange column (7 mm×60 cm). The praseodymium was eluted with $1M$ ammonium lactate at pH 3.75–3.85; the lanthanum was eluted at pH 3.95. The rare earth was separated from the eluant by precipitation at pH 4 with HF. The precipitate was dissolved in HNO_3 and HBO_3 as before and reprecipitated as the hydroxide. After dissolving in dilute HCl, it was precipitated as an oxalate, filtered, dried, and placed on an aluminum card for counting.

2. Cerium Targets

After irradiation, the aluminum backings of the targets were dissolved in dilute HCl. The solutions, which also contained the undissolved CeO_2, were evaporated carefully to dryness; concentrated H_2SO_4 was added and the solution was boiled, thereby converting $AlCl_3$ to $Al_2(SO_4)_3$ and CeO_2 to $Ce(SO_4)_2$. The $Ce(SO_4)_2$ was dissolved in H_2O, made up to volume in a volumetric flask, and an aliquot of this solution was subsequently analyzed for Ce^{4+} content. Sodium and praseodymium carriers were then added to the remaining solution. H_2O_2 was used to reduce Ce^{4+} to Ce^{3+}, concentrated HF was added at pH 5 to achieve the precipitation of CeF_3 and PrF_3, and the cerium and praseodymium fractions were then purified and separated from each other in the same way as just described for the lanthanum targets.

To the aqueous phase from the cerium-praseodymium separation, H_2O_2 was added to reduce the higher oxidation state of silver to Ag^+, followed by NH_4OH to precipitate the $Pr(OH)_3$. The precipitate was washed, dissolved in 1 cc of dilute HCl, and precipitated as oxalate. The precipitate was filtered, dried, and placed on an aluminum card for counting.

3. Chemical Yield Determination

The rare earths were analyzed spectrophotometrically as the complex with arsenazo [3-(2 arsonophenylazo)-4, 5-dihydroxy-2, 7-naphthalene-disulfonic acid][32] at pH 8.0.

[32] J. S. Fritz, M. J. Richard, and W. J. Lane, Anal. Chem. **30**, 1776 (1958).